



Synthesis and characterization of carboxymethyl cellulose based hydrogel and its applications on water treatment

Aisha Hameed*, Shazia Khurshid, Ahmad Adnan

Government College University Lahore, Pakistan, Tel. +92 300 8083203; email: aishahameed09@gmail.com (A. Hameed), Tel. +92-0333-4282231; email: shaziakhurshid1@yahoo.com (S. Khurshid), Tel. +92 111-000-010/+92 042-35304092, Ext. 262; email: ahmadadnan@gcu.edu.pk (A. Adnan)

Received 26 September 2019; Accepted 26 April 2020

ABSTRACT

The synthesis of carboxymethyl cellulose/potato starch/amyllum starch-based hydrogel was done by using aluminum sulfate octahydrate as a cross-linking agent. The novel hydrogel was then investigated and characterized by studying different parameters like swelling behavior, swelling kinetics, scanning electron microscopy (SEM), Fourier transform infrared (FT-IR), powdered X-ray diffractometry, and thermogravimetric analysis (TGA). This novel hydrogel was applied to tap water for the removal of heavy metal ions which are health hazardous for human life. Among all these mentioned above, the FT-IR analysis was done primarily to evaluate the structure of hydrogels. The resulting structures were in accordance with the expected structures of hydrogels. These hydrogels were then analyzed by the TGA in order to evaluate the thermal stability of hydrogel which should be more than its ingredients. After the thermal gravimetric analysis, these hydrogels were then examined morphologically by SEM. The swelling ability of the prepared hydrogel was examined in the basic medium as well as in the acidic medium. Resultantly it was found to be more in proportion in the basic medium than in acidic medium. Moreover, the hydrogel shows its swelling and de-swelling behaviors in different solvents like water, ethanol, acidic, and basic buffers and also in salt solutions when inferred by the swelling experiments. By the application of the prepared hydrogel on the aqueous solutions, Cd^{2+} , Pb^{2+} , and Fe^{2+} ions were separated. The order of selectivity of the hydrogel toward different metal ions was found to be $\text{Cd}^{2+} > \text{Pb}^{2+} > \text{Fe}^{2+}$. It can be inferred that the capacity of the hydrogel to bind with heavy metal ions depends upon the interaction of different metal ions with the hydrogel monomers.

Keywords: Superabsorbent polymers; Carbohydrate based polymers; Biomedical applications; Metal ion removing capability

1. Introduction

A hydrogel can be defined specifically as a substance consists of hydrophilic polymers arranged in a three-dimensional pattern to form a network. The wide range of applications of a hydrogel is attributed to its ability to absorb a large amount of water by swelling up and keeping its structure retained. It is all due to its cross-linked structure with solutions or water molecules and this fact

was reported firstly by Wichterle and Lim [1]. A hydrogel normally contains 10% water of its weight. The hydrogels possess relatively high grade flexibility because of their high water contents like natural tissues. Moreover, hydrogels may show a hydrophilic property because of the presence of some hydrophilic groups ($-\text{COOH}$, $-\text{NH}_2$, $-\text{OH}$, $-\text{CONH}_2$, and SO_3H [1]). On the basis of their flow behavior, they can be categorized into weak and strong hydrogels [2]. Because of

* Corresponding author.

the wide range of their applications, they're also used in the food industry, that is, some edible gels are used as gelling polysaccharides at a large scale [3]. In short, the term hydrogel may be described as a structure of three-dimensional network with cross-linked molecules. Irrespective of their source, either obtained from synthetic or natural class of polymers, they contain similar property of swelling up by absorbing a significant amount of water [4].

Heavy metal pollution is considered as one of the serious environmental hazards not only for human beings but also for all living organisms due to its toxic and carcinogenic effects. In recent years, methods like ion exchange, chemical precipitation, membranous separation, and adsorption have been employed to reduce such a type of environmental pollution. Due to its economic and technical applications among all the above-discussed methods, the most reliable choice to reduce this type of pollution is the method of adsorption [5–8].

Human activities like mining, smelting, alloy manufacturing, textile operations, use of pesticides, fertilizers, electronics, and paint industry, resultantly cause cadmium (Cd^{2+}), iron (Fe^{2+}), and lead (Pb^{2+}) to accumulate these highly toxic environmental pollutants in the groundwater reservoirs [9–12]. Almost all these above-mentioned activities can also result in the accumulation of heavy metals in the environment and ultimately these metals penetrate in the living tissues and become a part of the food chain [13]. High levels of these metal ions in the human body can lead to some serious and major problems, that is, cancer [14,15], kidney dysfunction, prostate carcinogenesis [16], multiple bone fractures, hypertension [17], and weight loss [18]. Some cellulosic materials such as agriculture waste [19,20] and carboxylated cellulose nano-crystals [20], fruit peels and plant barks [21] (low-cost sorbents) are reported to depict a relatively high capability for metal binding and removal of heavy metal ions and they can be considered useful as they are abundant and renewable sources in nature. In view of above-described hazards, there arises an increased need of an efficient method with a high and defined sorption capacity with a specific type of functional group preferably. Among all the renewable biopolymers occurring naturally, cellulose possesses some modifiable hydroxyl groups [22]. By modifying these hydroxyl groups and grafting the polysaccharides on the resulting carboxylate group, the exchange of cations in aqueous solutions can be made possible [23].

Therefore, by chemically modifying the substances containing cellulose/ polysaccharide structures, we can enhance its ability to uptake of metal ions from the solution. Synthesis of a super-absorbent hydrogel by commercially available low-cost polysaccharide, that is, carboxymethyl cellulose (CMC), combined with other starch, that is, potato and amylose starch (PS/AS) was studied extensively in the following described experiments. Moreover, the cross-linked polymer complexes (CMC) associated with aluminum ions by non-permanent chemical bonds were also studied, when further observed in the presence of water, which showed their swelling behavior. These cross-linked starch and CMC can create an environment-friendly biopolymer-based SAP which may help to reduce the hazardous metal ions from human consumption substances [23].

2. Materials and methods

The commercially available powders of PS (laboratory grade), AS (laboratory-grade with no further purification), and sodium salt of CMC were purchased from a scientific store located in Lahore, Pakistan (average molecular weight = 90,000) (DS = 0.7). The CMC along with these starches was used for the synthesis of superabsorbent polymers (SAP) [24]. To crosslink the polymer complex, aluminum sulfate octadecahydrate (reagent grade) was also used [25].

2.1. Preparation of superabsorbent polymer

By using a magnetic stirrer in a large beaker, about 20 g of sodium salt of CMC was mixed with distilled water (2.0 L). Soon after the mixing, these two starch types (1.2 g) were subjected to gelatinization at 80°C in distilled water (50 mL) for 45 min. In CMC solution, previously gelatinized starch was added and they were allowed to mix for 1 h. Aluminum sulfate in some variable amounts was then introduced into the beaker for another 30 min and the whole mixture was allowed to mix thoroughly. The whole solution was placed on Teflon baking pans and dried at 70°C until the formation of a film. With the help of a blender and pestle mortar, the film was shredded and grinded into a powder respectively [26,27]. Soon after the addition of more than 2.3% of Aluminum sulfate, the polymer exhibited an over-crosslinked complex. The resulting complex develops into a structure carrying a lot of connections rendering too small voids for optimal water absorbency [28].

3. Characterizations

3.1. Flow-ability parameters of SAP

3.1.1. Angle of repose

Fixed funnel method was used to find out the angle of repose for the purpose of studying the flow property of hydrogel [29]. Through a fixed funnel placed previously on a graph paper, hydrogel (powdered) was then allowed to fall. Angle of repose (θ) was calculated by the following equation:

$$\tan\theta = \frac{h}{r} \quad (1)$$

where h is the height of heap; r is the radius of heap.

3.1.2. Bulk and tap density

By the placement of the hydrogel (1.0 g) in graduated cylinder, we can measure the volume of hydrogel V_b . The tapped volume (V_t) was noted after tapping 100 times the graduated cylinder. Tap density (D_t) and bulk density (D_b) were calculated by using Eqs. (2) and (3), respectively:

$$D_t = \frac{\text{Weight of Hydrogel}}{\text{Volume of Hydrogel } (V_t)} \quad (2)$$

$$D_b = \frac{\text{Weight of Hydrogel}}{\text{Volume of Hydrogel } (V_b)} \quad (3)$$

3.1.3. Hausner ratio and Carr's index

The specific hydrogel's flow properties can be determined by means of Hausner ratio and Carr's index [29]. "Hausner ratio is the ratio of tap density to bulk density" as mentioned in Eq. (4):

$$\text{Hausner ratio } (h) = \frac{D_t}{D_b} \quad (4)$$

"Carr's index is the percentage ratio which represents arrangement of particles" and it can be measured by using Eq. (5):

$$\text{Carr's index } (C) = 100 \times \left(1 - \frac{D_t}{D_b} \right) \quad (5)$$

where D_b and D_t are bulk and tap densities, respectively.

3.1.4. Moisture content

Before and after drying, the weight of hydrogel was calculated at 105°C (1 h).

3.1.5. Centrifuge retention capacity

"Water retention capacity is the ratio of wet sediment mass to dried mass." Centrifuge retention capacity or water retention capacity was measured by centrifuging the freshly prepared solution of hydrogel (1% w/w) at 4,500 rpm (30 min) in deionized water at 25°C. Weight of wet paste was measured after decanting the supernatant. Weight of the dried mass was checked after completely drying the paste at 70°C [30,31].

3.1.6. Swelling capacity

The tapped volume was measured by tapping the graduated cylinder 100 times in which the powdered hydrogel (1.0 g) was placed. Then, in de-ionized water, hydrogel was mixed thoroughly and the volume was adjusted to 100 cm³. After keeping for 24 h of these swollen hydrogel's sediment, its volume was observed and swelling capacity (v/v) was calculated by using Eq. (6):

$$\text{Swelling Capacity } (v/v) = \frac{\text{Swollen Volume}}{\text{Tapped Volume}} \quad (6)$$

3.1.7. Dynamic and equilibrium swelling

In order to find out the pH dependent swelling, SAP (0.1 g each) were placed in the bags of cellophane which were soaked into phosphate buffers (pH 6.8 and 7.4), HCl buffer (pH 1.2) and deionized water for 24 h. The weights of these swollen hydrogels were checked after regular

intervals for 24 h. The swelling capacity (g/g) in each case was calculated as:

$$\text{Swelling Capacity } (g/g) = \frac{W_t - W_0 - W_c}{W_0} \quad (7)$$

where W_t is the weight of swollen hydrogel (with wet cellophane bag), W_0 is the weight of dry hydrogel, and W_c is the weight of wet cellophane bag.

The normalized degree of swelling (Q_t) is a ratio between media (buffers of pH 1.2, 6.8, 7.4, and de-ionized water) penetrated into gel and initial weight of hydrogel at time t as given in Eq. (8).

$$Q_t = \frac{W_s - W_d}{W_d} = \frac{W_t}{W_d} \quad (8)$$

where W_s is the weight of swollen hydrogel at time t , W_d is the weight of dried hydrogel at time $t = 0$, W_t is the weight of water penetrated into hydrogel at time t , Q_e is the (normalized equilibrium degree of swelling) is the ratio of media penetrated into hydrogel at t_∞ to weight of dried hydrogel at $t = 0$. It can be calculated by Eq. (9):

$$Q_e = \frac{W_\infty - W_d}{W_d} = \frac{W_e}{W_d} \quad (9)$$

where W_∞ is the weight of swollen hydrogel at time t_∞ (swelling remains constant), W_d is the weight of dried hydrogel ($t = 0$), W_e is the amount of water absorbed by hydrogel (t_∞).

3.1.8. Swelling kinetics

To find out the kinetic order of swelling, normalized degree of swelling (Q_t) and normalized equilibrium degree of swelling (Q_e) values can be used [32]. The second-order kinetics Eq. (10) can be calculated by using the following equation [33]:

$$\frac{t}{Q_t} = \frac{1}{KQ_e^2} + \frac{t}{Q_e} \quad (10)$$

3.1.9. Swelling and de-swelling behavior in response to external stimuli

SAP has ability to show swelling and de swelling in different aqueous and non-aqueous media. The Gravimetric method was employed for its analysis.

- The swelling of hydrogel was observed while keeping its cellophane bag (0.1 g) in deionized water, allowed to stand for 1 h and its weight was measured. Then by placing it in pure ethanol for 1 h, its weight was again measured as a function of its de-swelling time.
- By using buffer solutions (pH 7.4 and 1.2), the swelling and de-swelling behaviors were studied in another experiment. The swelling was observed by keeping its

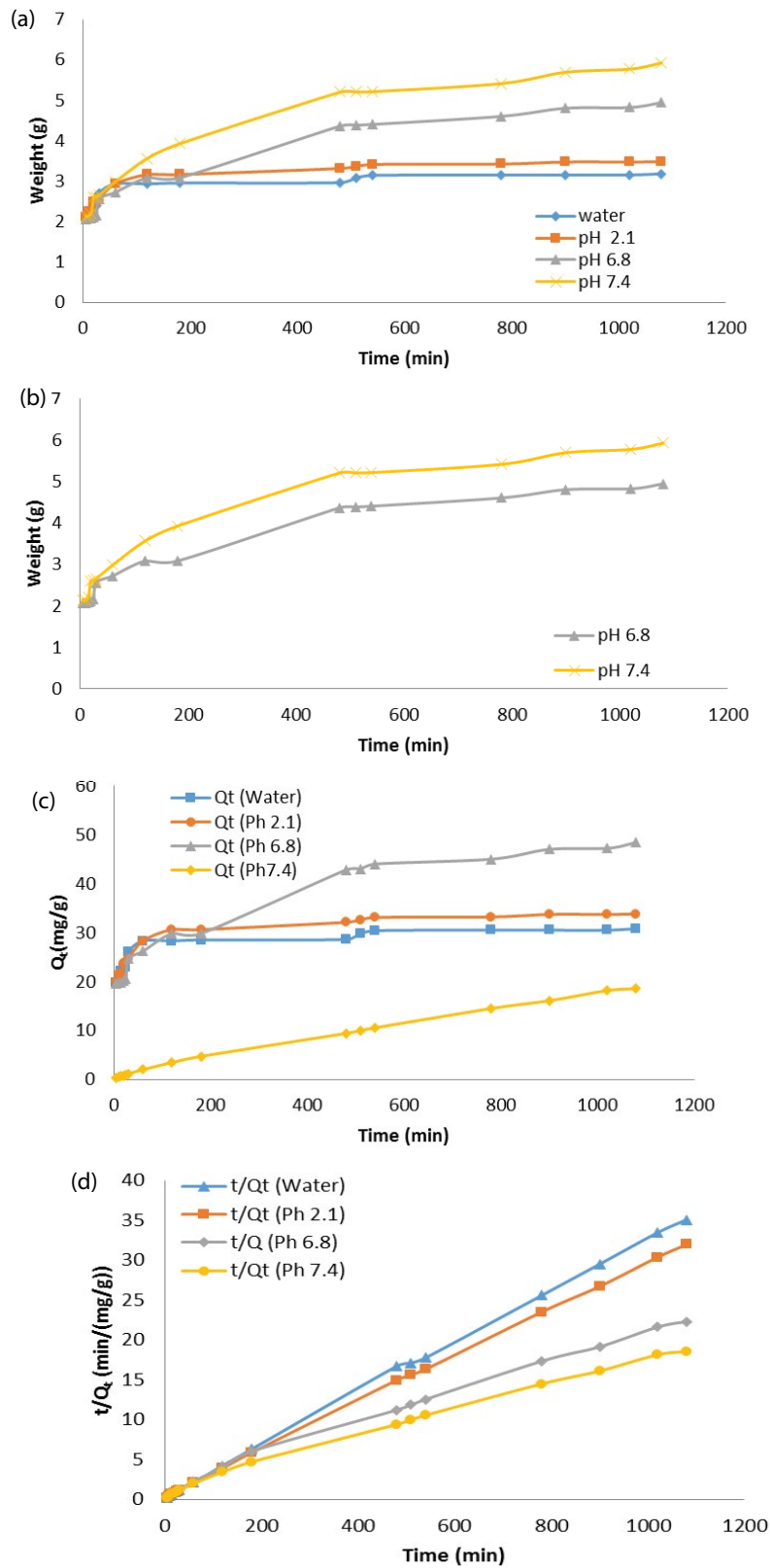


Fig. 1. (a) Swelling data of SAP obtained in water and buffers of pH 1.2, 6.8, and 7.4 and (b) swelling data and kinetics of SAP obtained in buffers of pH 6.8 and 7.4. From the swelling data, the values of Q_t (mg/g) and t/Q_t (min/(mg/g)) were found out, and were plotted against the time (min). (c) swelling data of SAP between time (min) and Q_t (mg/g) obtained in water and buffers of pH 1.2, 6.8, and 7.4. (d) swelling data of SAP between time (min) and t/Q_t (min/(mg/g)) obtained in water and buffers of pH 1.2, 6.8, and 7.4.

cellophane bag (0.1 g) in a buffer (pH 7.4) for 1 h and after that its de-swelling was observed by keeping in another buffer solution (pH 1.2) for 1 more hour.

- As above mentioned, the swelling and de-swelling behavior was also observed in water and aqueous NaCl solution (0.9%).

As decrease in the osmotic pressure occurs due to addition of salt between hydrogel and water, similar phenomenon happens in the present case and the swelling decreases and vice versa. In other words de-swelling occurs due to the fact that water molecules moves out of hydrogel rendering it flaccid [34,35].

3.2. Scanning electron microscopy

The internal structure and superficial morphology of SAP were analyzed by a 10 kV operating scanning electron microscope (NanoSEM 450, Field Electron and Ion Company Nova). In deionized water (2 mL), dried hydrogel (0.1 g) was allowed to mix by mixer mill. This mixture was subjected to sonication for 30 min in order to remove air bubbles from it. Then, resulting swollen SAP was placed at -20°C , allowing it to get frozen and was subjected to freeze-drying. Moreover, sharp blade was used to get the cross-sections of hydrogel transversely and vertically to reveal its porous nature.

3.3. FTIR analysis

Fourier transform infrared spectroscopy (FT-IR, KBr, $4,000\text{--}400\text{ cm}^{-1}$) was performed on CMC sodium (CMC.Na), potato, amyllum starches, and SAP by using an IR-Prestige-21 instrument (Shimadzu Corporation, Kyoto, Japan). The obtained spectra by FT-IR were measured.

3.4. Powdered X-ray diffraction analysis

Powdered X-ray diffractometry (PXRD) of all four samples was performed under the given conditions.

3.5. Thermogravimetric analysis

Thermogravimetric analysis (TGA) was performed on all four samples, that is, CMC sodium (CMC.Na), potato, amyllum starches, and SAP. On the basis of results obtained from the above-said method, the maximum and final thermal decomposition temperatures were investigated. The obtained data was analyzed by using Universal Analysis 2000 and Microsoft Excel 2010 software.

4. Applications

4.1. Atomic absorption spectroscopy

To get the optimized amount, the 10, 20, 40, 60, 80, and 100 mg of SAP was used to add in 100 mg/L solutions of Cd^{2+} , Pb^{2+} , Fe^{2+} , and then stirred at the temperature of 298 K, at the rate of 130 rpm for 30 min. The samples were analyzed on flame atomic absorption spectrophotometer, Shimadzu AA-7000F (Kyoto, Japan). All values of metal analysis were recorded in parts per million (ppm: mg/L). For the calibration curve, four standards, that is, 0.5, 1.0, 2.0, and 4.0 ppm were

Table 1

Conditions for powdered X-ray diffractometry (PXRD) of all four samples, that is, potato starch, amyllum starch, carboxy-methylcellulose and SAP

Anode material	Cu
Generator voltage	40
Tube current	40
Monochromator used	No
K-alpha1 wavelength	1.540598
K-alpha2 wavelength	1.544426
Ratio K-alpha2/K-alpha	0.5
File date and time	13-08-18 12:42
<i>h k l</i>	0 0 0
Scan type	Continuous
Scan axis	Gonio
Scan range	20–80
Scan step size	0.02
No. of points	3,000
Phi	0
Time per step	0.2

also used. To study the adsorption behavior, two empirical adsorption models named Freundlich and Langmuir models were used. The obtained experimental data at pH 7 was analyzed by applying Freundlich and Langmuir equations. The Freundlich and Langmuir isotherms are given by Eqs. (10) and (11), respectively.

where K_f is the Freundlich constants related to adsorption capacity, N is the Freundlich constants related to intensity, and C_e is the equilibrium concentration of metal ion in the solution.

$$\frac{C_e}{Q_e} = \frac{C_e}{Q_{\max}} + \frac{1}{bQ_{\max}} \quad (11)$$

where Q_{\max} and b are the Langmuir constants related to maximum monolayer adsorption capacity and adsorption energy.

5. Results and discussion

5.1. Physical properties of SAP

The physical properties of prepared hydrogel are as shown in Table 2.

Hausner ratio, Carr's index, and angle of repose are indicative of poor flow property of powdered SAP.

5.2. Swelling kinetics

5.2.1. pH responsive swelling of SAP

Buffers of pH 1.2, 6.8, and 7.4 were made according to the pH values of stomach, and the different parts of intestine, to check the swelling behavior of SAP upon them. The swelling behavior of hydrogel in deionized water was found to be more as compared to acidic and basic buffers (pH 1.2, 6.8, and 7.4). We can infer that it may be due to the protonation

Table 2

Observed FT-IR bands of all the four samples, that is, potato starch, amyllum starch, carboxymethylcellulose and SAP

Moisture content (%)	20 ± 0.20
Average particle size (µm)	≈228
Angle of repose	3 ± 0.25
Bulk density (g/cm ³)	0.8 ± 0.01
Tapped density (g/cm ³)	0.66 ± 0.01
Carr's index (%)	17.5 ± 1.50
Hausner ratio	0.825 ± 0.06
Swelling capacity on 24 h (g/g)	37.33 ± 2.00
Centrifuge retention capacity (%)	70 ± 1.11

of carboxylic groups, located at the terminal ends of polymer chains. The capability of anion formation of carboxylic acid increases as the pH rises in contrast with the alkaline media. Moreover in basic buffers, there appeared a relatively low swelling capacity in comparison to its behavior in deionized water. In alkaline media, the screening effect of excess cations may be responsible for this relatively low swelling capacity which stops the anion–anion repulsions due to carboxylate anion's shielding effect. According to the literature, many other hydrogels's water absorbent property depend upon their pH values [3,34]. As explained by second-order kinetic mode, the pH dependent swelling of hydrogel is controlled by the relaxation of polymer chain and diffusion of solvent [35]. The kinetic study that was performed on data obtained by the swelling behavior of SAP shown in buffers of pH 6.8 and 7.4 and in deionized water is given below. The adsorption of metal ions, that is, Cd²⁺, Fe²⁺ and Pb²⁺ in SAP can be graphically represented by plotting a graph between their C_e (mol/L) and Q_e (mol/L) values, as shown in Figs. 18–20.

In practical applications, a higher swelling rate is required as well as a higher swelling capacity. The swelling kinetics for the absorbents is significantly influenced by factors such as swelling capacity, size distribution of powder particles, specific size area, and composition of polymer.

5.2.2. Swelling and de-swelling kinetics in different solutions

5.2.2.1. Swelling and de-swelling behavior of SAP in water and ethanol

Due to the less affinity of ethanol with hydrogel than water, the hydrogels usually de-swells rapidly in ethanol

(Fig. 2). In contrast, the dielectric constant (24.55) and a low polarity of ethanol than that of water (80.40) are responsible for formation of hydrogen bonding to a lesser extent with ethanol. Moreover, a less dielectric constant causes a drop in swelling capacity, that is, de-swelling of the polymer and ionization of ionizable groups. The swelling of hydrogel after placing it again in water is probably due to the result of extensive hydrogen bonding with water and a swift wash out of ethanol molecules.

5.2.2.2. Swelling and de-swelling behavior of SAP in acidic and basic buffers

By using different types of buffers, swelling, and de-swelling behavior of hydrogel in acidic and basic media was evaluated. According to the observations, SAP swells in basic buffer (pH 7.4) whereas a de-swelling behavior was shown by the hydrogel in acidic buffer (pH 1.2). This swelling and de-swelling behavior of SAP was observed four times and the measurements of these experiments (off and on) were recorded in form of a graph as shown in Fig. 3.

5.2.2.3. Swelling and de-swelling behavior of SAP in NaCl solution and deionized water

By immersing SAP in water and sodium chloride (0.9%) solution, the swelling and de-swelling of SAP was observed respectively. When studied at regular intervals, SAP shows a swelling behavior in de-ionized water while shrinkage observed in the solution of NaCl (Fig. 4). Among hydrogel and water, the addition of salt causes a decrease in osmotic pressure making the water molecules moved out of hydrogel render it to shrink.

5.3. Scanning electron microscopy

In order to study the surface morphology and porosity of a dried SAP, scanning electron microscopy (SEM) was used. The presence of interconnected macropores were confirmed by the SEM photographs of transversely cut cross-sections of a hydrogel (Fig. 5) ranging the size of 228 µm. When analyzed by SEM, the longitudinal cross-sections of hydrogel, an inter-connected network of macropores were also observed in the form of macroporous tubes, through which the transfer of solvents and water takes place. By this investigation, we can expect, that SAP may be used for water treatment, diapers, cosmetics, pharmaceuticals, and controlled drug release.

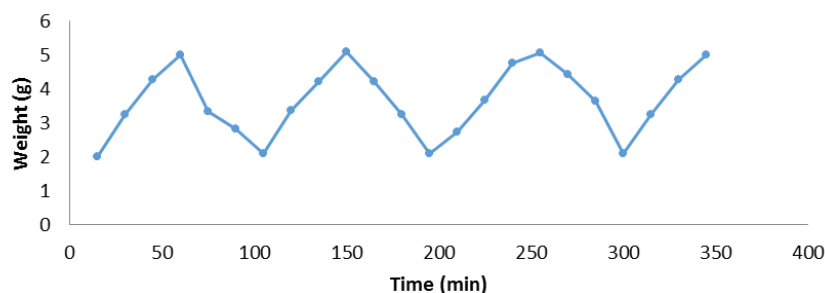


Fig. 2. Swelling and de-swelling of SAP in aqueous and ethanol media.

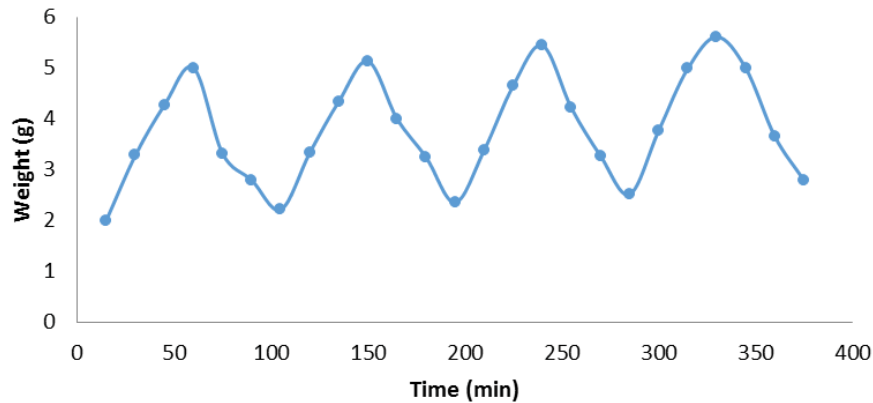


Fig. 3. Swelling and de-swelling behavior of SAP in acidic and basic buffers.

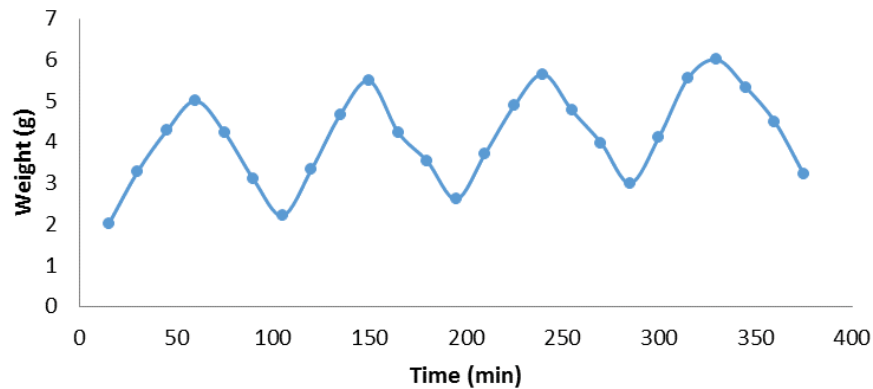


Fig. 4. Swelling–deswelling behavior of SAP in deionized water and 0.9% NaCl solution.

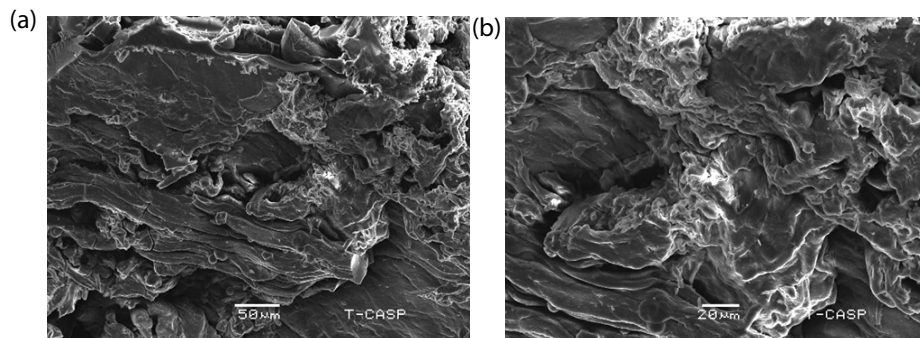


Fig. 5. Scanning electron micrographs of SAP with average pore size 228 μm at magnifications of (a and b) 50–20 μm .

Fig. 5 shows the magnified images of prepared hydrogel, in which empty spaces between gel folds can be seen clearly. The hydrophilic groups present in the empty spaces may have an ability to trap the smaller ions, for example, Fe^{2+} , Cd^{2+} , and Pb^{2+} .

5.4. Fourier transform infrared spectroscopy

FTIR was performed on all of the four samples, that is, CMC.Na, potato and amyllum starches, and SAP, respectively.

The absorption was observed at 3,270 cm^{-1} (hydroxyl stretch influenced by hydrogen bond), 1,569 and 1,388 cm^{-1}

(carbonyl stretch), 980 cm^{-1} (b-1,4-glycosidic bond) and 2,942 and 2,838 cm^{-1} (methylene), which were characteristic absorptions in cellulose and methylcellulose structures. The obtained FT-IR (KBr), by the analysis of potato, amyllum starches, CMC, and SAP are clearly shown in Figs. 6–10 in order to elaborate the desired modifications. The success of the reaction in the FT-IR spectrum of SAP was revealed by an ester carbonyl distinct signal's appearance at 2,000 cm^{-1} in spectra of CMC which was the major constituent of hydrogel, jumps to a relatively higher wavenumber at 2,812 cm^{-1} soon after the formation of its SAP. It also indicates the absorption of carbon dioxide at the time of completion of reaction. In addition. The salt

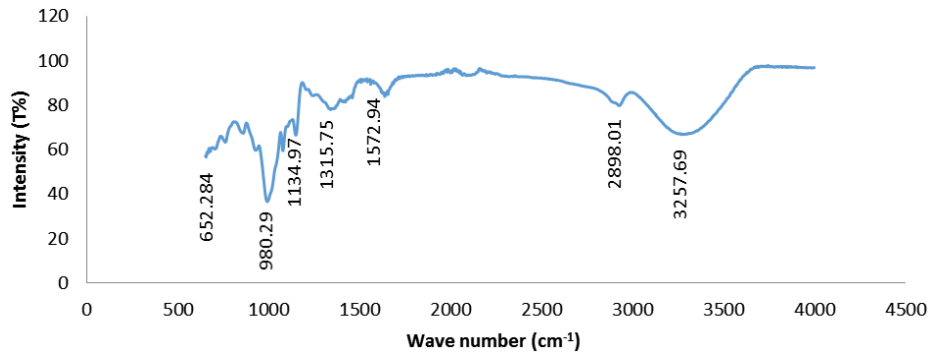


Fig. 6. FTIR spectra of potato starch.

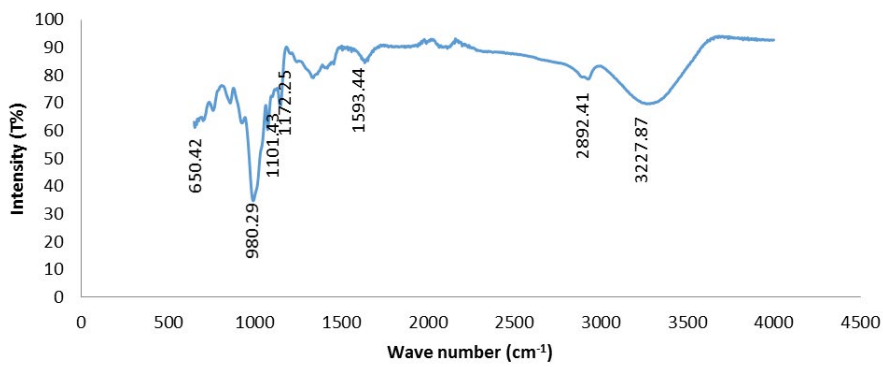


Fig. 7. FTIR spectra of amyllum starch.

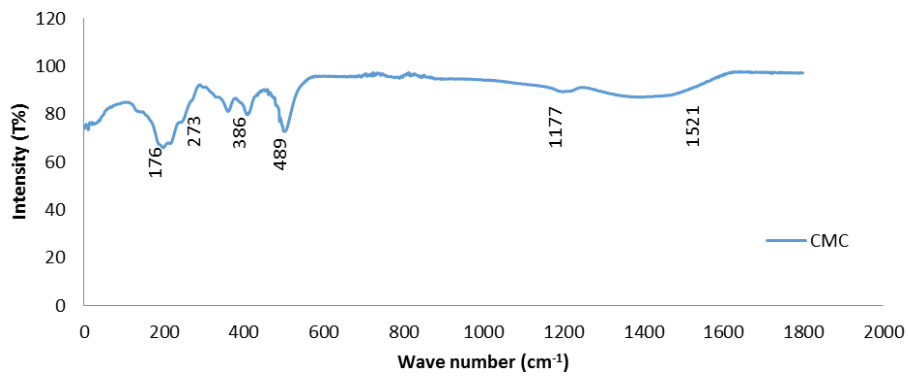


Fig. 8. FTIR spectra of carboxymethyl cellulose.

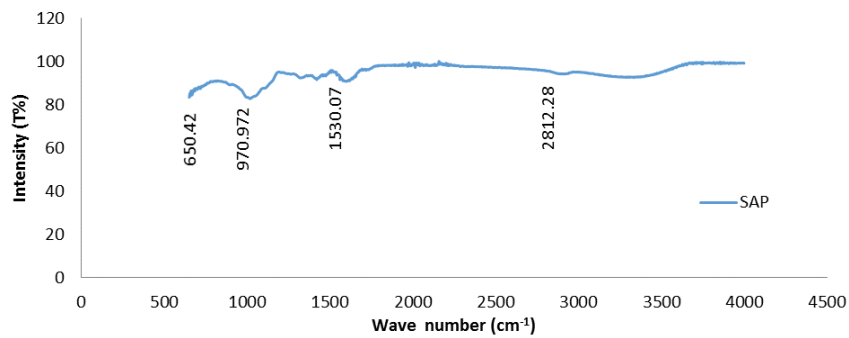


Fig. 9. FTIR spectra of SAP.

Table 3
Observed FT-IR bands and their assignments

Material	v(O-H)	v(C-H) aliphatic	HOH deformation	$\delta(\text{O-H})$ Inplane	$\delta(\text{CH}_2)$	$\delta(\text{CH})$	δ_{ASYM} bridged oxygen	v(C-O-C)	V(C-C) arabinosyl side chain	δ_{ASYM} (out of plane β -glycosidic bond)	Polymer backbone	Unassigned
Potato starch	3,134; 3,560	2,960	1,649	-	1,421	1,350	1,240	1,070	-	995,923,852	653,605	1,139; 2,140
Amylum Starch	3,466; 3,487	2,904	1,641	-	1,427	1,350; 1,338	-	-	1,010	952,850	651,553	1,132; 2,904
Carboxymethyl cellulose	3,552	2,885	1,597	1,462	-	-	-	1,066	-	916	648,590	704
Modified Starch	3,209	2,877	1,681	-	1,409	-	-	-	1,001	999,931,860	661,559	2,175; 1,132
SAP	3,444; 3,361	2,879	1,602	-	1,427	1,336	-	1,066	-	985,927,879	665,586	833,665
MSAP	3,585	2,881	1,645	-	1,417	1,327	-	-	1,001	912	663,570	1,525

formation can be indicated by the absorption of carboxylate ion in the spectrum from 460 cm^{-1} of CMC to 464 cm^{-1} of SAP.

5.4.1. Observed FT-IR bands and their assignments

5.5. PXRD analysis

Some very clear and sharp diffraction signals can be seen at 28, 33, 38, 45, 68, 70, 74, and 80 in the CMC's diffractogram by X-ray diffraction (XRD) method (Figs. 11–14), which are actually a characteristic of cellulose. In contrast, these diffraction signals at 28, 33, 38, 45, 68, 70, 74, and 80 were not observed in the XRD diffractogram of SAP, only some peaks at 38, 67, and 68 were observed, that is, there may be a distortion in the CMC's crystallization and an increase in SAP hydrogel's amorphous region. Its possible cause may be the chemical crosslinking between the starches, CMC, and SAP. These results indicate a reduction in the crystalline behavior during the gel formation and resultantly metal ions can easily penetrate into the hydrogel folds. In view of the above description, we can say that the SAP hydrogel beads may have a relatively high tendency for metal ions absorption. The maximum intensity of peaks of potato starch, Amylum, CMC were at 127, 156, and 56, respectively while that of SAP was at 128 represents the crosslinking between both starches and CMC, however, the diffraction peaks have completely vanished in case of SAP. Thus, we can reasonably assume the reason lying behind, that is, the formation of co-ordination bonds of hydrogel with the carboxyl groups of CMC and starches.

5.6. Thermogravimetric analysis

The thermal analysis of potato starch, amyllum starch, CMC-Na, and SAP were recorded for comparison. Figs. 15 and 16 show an overlying pattern of the TG Curves of all the ingredients and SAP, and a straight line for the decomposition of SAP. The minimum degradation (T_{d_m}) in SAP's first degradation step appeared at 231.46°C , which is slightly higher than the T_{d_m} of both starches whereas less than that of CMC-Na. Likewise, T_{d_i} of SAP's second degradation step was 596°C and almost 35°C higher than starches whereas equal to that of CMC-Na. In the last degradation step, with the remaining weight of 21.97%, a complete decomposition of the starches were observed. From major degradation steps, the obtained thermal data reveals a significantly higher values of T_{d_v} , T_{d_m} , and T_{d_f} of SAP as compared to its ingredients. As observed throughout the TG curves, we may infer an extraordinary thermal stability of the sorbent. In order to increase the sorbent's shelf life, this increase in thermal stability can be used as a beneficial tool especially for commercial applications.

By analyzing the thermal analysis of SAP's major degradation steps above 200°C , we can conclude that the SAP possesses a relatively higher thermal stability as indicated in graph given below. This increase in thermal stability can be helpful for the purpose of increasing the sorbent's shelf-life, suggesting its future use in some commercial applications.

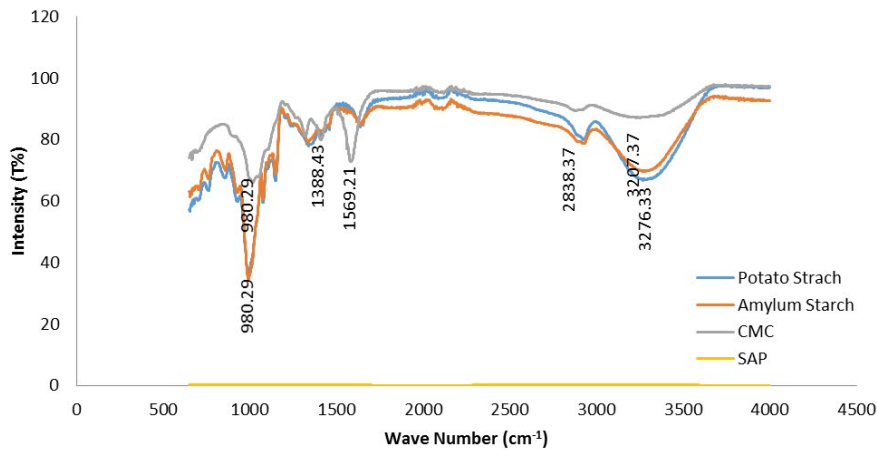


Fig. 10. Combined FTIR spectra of potato, amyllum starches, CMC, and SAP.

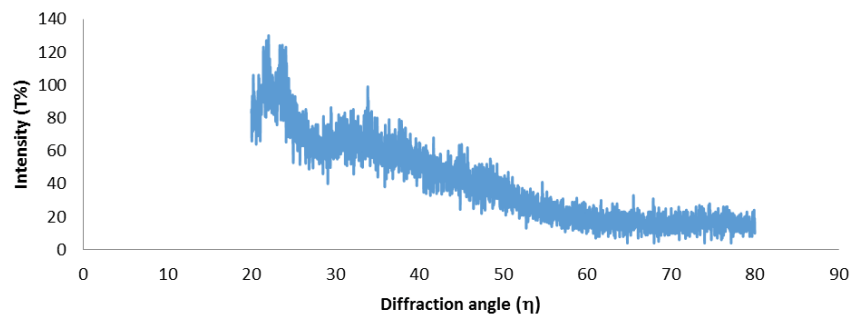


Fig. 11. PXRD analysis of potato starch.

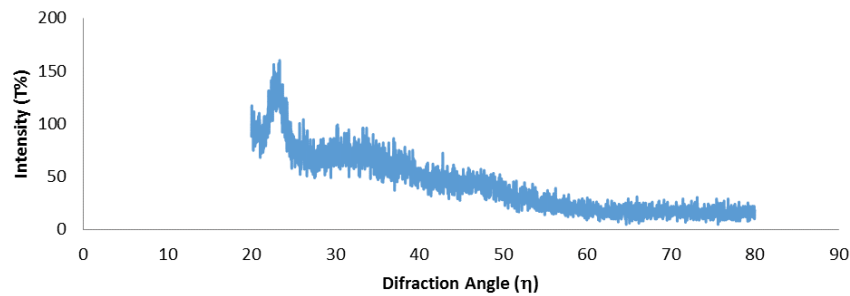


Fig. 12. PXRD analysis of amyllum starch.

6. Applications

6.1. Atomic absorption spectroscopy

The Fig. 17 shows the metal ion absorption rates in the SAP solution. An increase in the concentration of SAP results an increase in the adsorbed quantity of metal ions. The 14, 12, and 10 ppm concentration for Cd²⁺, Pb²⁺, and Fe²⁺ indicates maximum absorption respectively. In fact, a relatively stronger attraction of oxygen atom of carboxyl group is the reason for an increased absorption rate of Cd²⁺ ion than other metal ions, which is helpful in reaction with Cd(II), Fe(II), or Pb(II) forming a relatively stable complexes with Cd(II) [36]. When the concentration of metal ions get lower than 0.2 mmol/L, the absorption ratio for Fe(II)

exceeds to 95%, and the absorption percentage for Cd(II) and Pb(II) becomes higher than 99%. An increase in the concentration causes the adsorption ratio to decrease and a better adsorption capacity was seen by hydrogel for the metals under consideration, hence we can infer a relatively higher adsorption capacity of the SAP hydrogel beads, so the hydrogel can be taken into consideration for the recovery of metal ions from solutions.

6.2. Adsorption isotherms

To study the adsorption behavior, two empirical adsorption models named Freundlich and Langmuir models were used. In this work, the analysis was done by applying

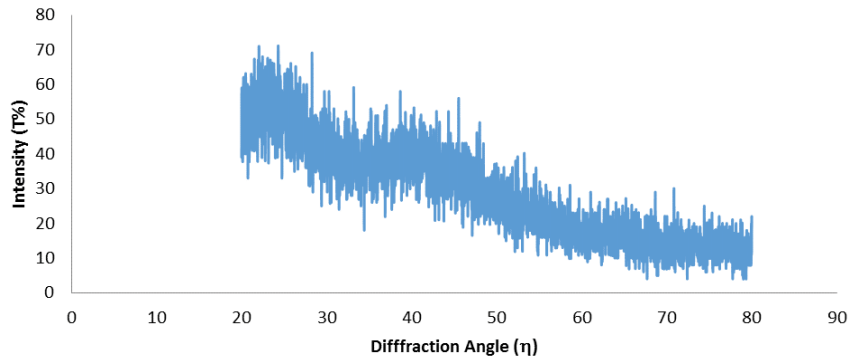


Fig. 13. PXR analysis of carboxymethyl cellulose-sodium.

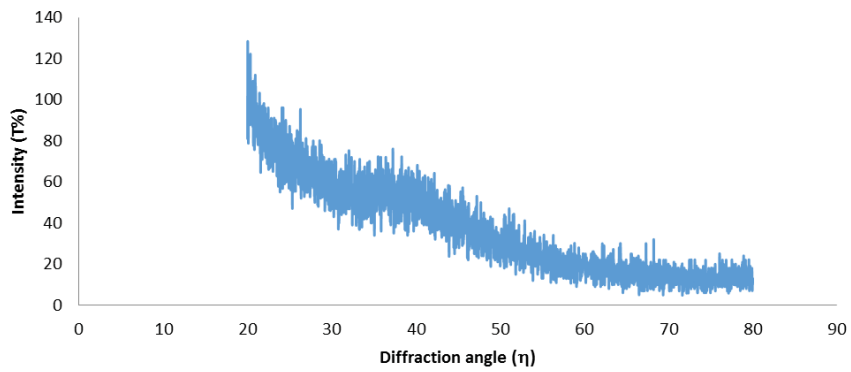


Fig. 14. PXR analysis of SAP.

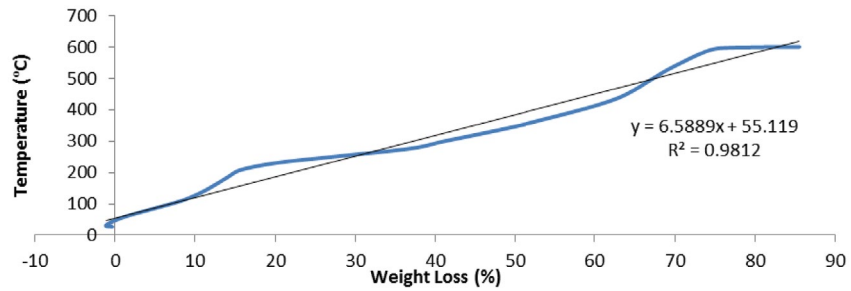


Fig. 15. Overlying graph of thermo-gravimetric (TG) straight line of SAP, indicating thermal stability of sorbent.

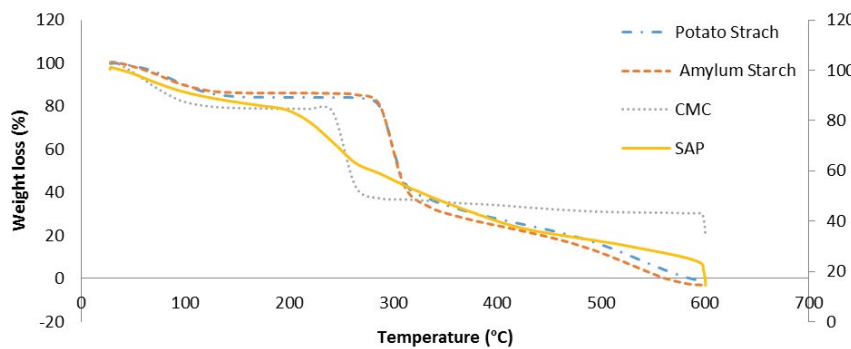


Fig. 16. PXR analysis of potato, amyllum starchces, carboxymethyl cellulose sodium, and SAP.

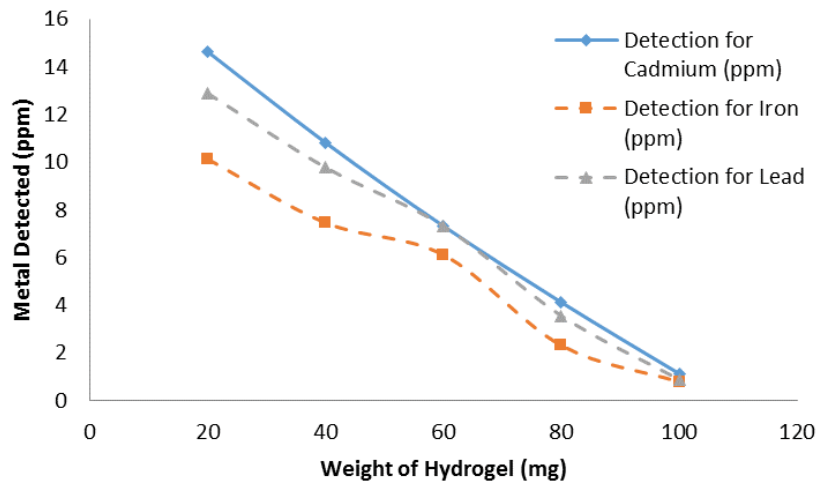


Fig. 17. Metal ion adsorption capacity of SAP at room temperature.

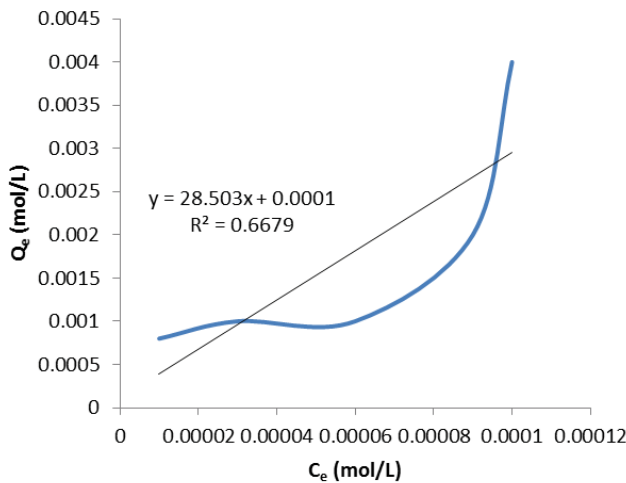


Fig. 18. Graphical representation of cadmium ion absorption in SAP between C_e (mol/L) and Q_e (mol/L).

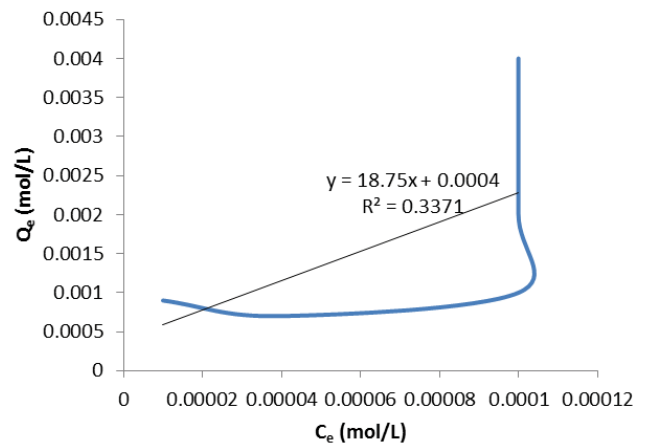


Fig. 19. Graphical representation of Fe^{2+} ion absorption in SAP between C_e (mol/L) and Q_e (mol/L).

Freundlich and Langmuir equations on the experimental data obtained at pH 7. The Freundlich and Langmuir isotherms are given by Eqs. (11) and (12), respectively:

$$\text{Log } Q_e = \text{log } K_F + \frac{1}{n} \text{log } C_e \quad (12)$$

Adsorption isotherms describe how adsorbates interact with adsorbents and are of much importance for optimizing use of adsorbents. In this study, the Langmuir isotherm and Freundlich isotherm were used for analysis of results. Table 4 shows that the Langmuir isotherm poorly shows the adsorption of metal ions by the SAP as compared to Freundlich isotherms:

From Freundlich equation, the observed K_F values for Cd^{2+} , Fe^{2+} , and Pb^{2+} are 1.63, 1.008, and 1.57 for SAP, respectively. The adsorption studies demonstrate that the hydrogel can have a potential application in removal and recovery of heavy metal ions from wastewater.

7. Conclusion

A high swelling behavior was shown by SAP in deionized water, at pH 6.8 and 7.4 while no remarkable swelling at pH 1.2 was observed. Furthermore, its potential as an advanced drug delivery system was also confirmed by a remarkable swelling and de-swelling behavior of SAP in water and ethanol, in acidic (pH 1.2) and basic (pH 7.4) media and in water and normal saline solution. The FT-IR spectrum of SAP, the appearance of a distinct ester carbonyl signal at $2,000 \text{ cm}^{-1}$ in spectra of CMC (the major constituent of hydrogel), moved to higher wave number at $2,812 \text{ cm}^{-1}$ after its SAP formation revealed the success of the reaction. The macroporous nature of dried hydrogel by SEM analysis predicts its superabsorbent nature. SAP proves itself not only a potential candidate for water treatment, but also an effective substance in targeted and sustained delivery of drugs in colon and small intestine on the basis of its higher adsorption quality in basic media. XRD spectra revealed a lower crystalline property of hydrogel beads as compared to pure

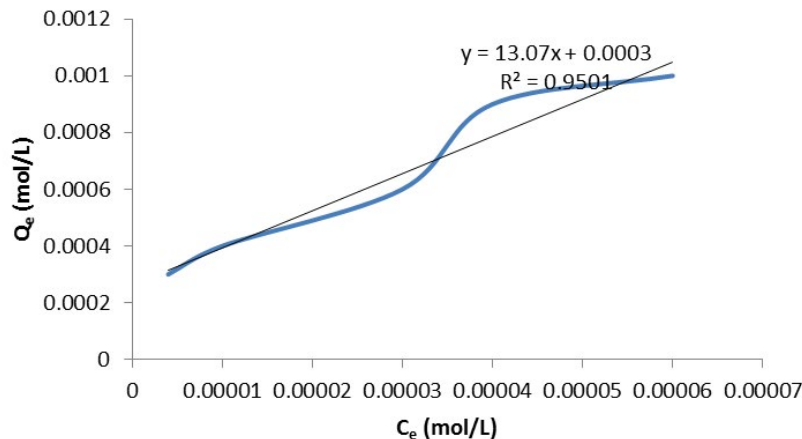


Fig. 20. Graphical representation of Pb^{2+} ion absorption in SAP between C_e (mol/L) and Q_e (mol/L).

Table 4
Freundlich and Langmuir equation fitted parameters

Freundlich equation	Metal ions	K_f	n	R^2
SAP	Cd^{2+}	1.63	1.85	0.898
	Fe^{2+}	1.008	0.88	0.798
	Pb^{2+}	1.57	2.22	0.955
Langmuir equation	Metal Ions	Q_{max}	b	R^2
SAP	Cd^{2+}	222	0.095	0.923
	Fe^{2+}	476	0.026	0.882
	Pb^{2+}	84	0.16	0.716

CMC. It is proved that the initial, middle, and final Thermal degradation steps of SAP are higher than the ingredient's data of degradation steps. It infers that the SAP has extraordinary thermal stability which can be observed throughout the TG curves. In view of the whole study, it is concluded that this hydrogel shows selectivity toward the absorption of metal ions, and finally can be recovered. The observed K_f values for Cd^{2+} , Fe^{2+} , and Pb^{2+} are 1.63, 1.008, and 1.57 for SAP, respectively. The adsorption studies demonstrate that SAP has a potential application in the removal and recovery of heavy metal ions from wastewater.

References

- [1] O. Wichterle, D. Lim, Hydrophilic gels for biological use, *Nature*, 185 (1960) 117–118.
- [2] J.D. Ferry, *Viscoelastic Properties of Polymers*, John Wiley & Sons, New York, 1980.
- [3] G. Pass, G. Phillips, D. Wedlock, Interaction of univalent and divalent cations with carrageenans in aqueous solution, *Macromolecules*, 10 (1977) 197–201.
- [4] J.M. Rosiak, F. Yoshii, Hydrogels and their medical applications, *Nucl. Instrum. Methods Phys. Res., Sect. B*, 151 (1999) 56–64.
- [5] Q. Zhu, Z. Li, Hydrogel-supported nanosized hydrous manganese dioxide: synthesis, characterization, and adsorption behavior study for Pb^{2+} , Cu^{2+} , Cd^{2+} and Ni^{2+} removal from water, *Chem. Eng. J.*, 281 (2015) 69–80.
- [6] T.E. Dudu, M. Sahiner, D. Alpaslan, S. Demirci, N. Aktas, Removal of $As(V)$, $Cr(III)$ and $Cr(VI)$ from aqueous environments by poly (acrylonitril-co-acrylamidopropyl-trimethyl ammonium chloride)-based hydrogels, *J. Environ. Manage.*, 161 (2015) 243–251.
- [7] R. Hua, Z. Li, Sulfhydryl functionalized hydrogel with magnetism: synthesis, characterization, and adsorption behavior study for heavy metal removal, *Chem. Eng. J.*, 249 (2014) 189–200.
- [8] P. Souda, L. Sreejith, Magnetic hydrogel for better adsorption of heavy metals from aqueous solutions, *J. Environ. Chem. Eng.*, 3 (2015) 1882–1891.
- [9] T. Nguyen, H. Ngo, W. Guo, J. Zhang, S. Liang, Q. Yue, Q. Li, T. Nguyen, Applicability of agricultural waste and by-products for adsorptive removal of heavy metals from wastewater, *Bioresour. Technol.*, 148 (2013) 574–585.
- [10] L. Yan, Y. Huang, J. Cui, C. Jing, Simultaneous $As(III)$ and Cd removal from copper smelting wastewater using granular TiO_2 columns, *Water Res.*, 68 (2015) 572–579.
- [11] J. Duan, J. Tan, J. Hao, F. Chai, Size distribution, characteristics and sources of heavy metals in haze episod in Beijing, *J. Environ. Sci.*, 26 (2014) 189–196.
- [12] T. Liu, X. Yang, Z.-L. Wang, X. Yan, Enhanced chitosan beads-supported FeO -nanoparticles for removal of heavy metals from electroplating wastewater in permeable reactive barriers, *Water Res.*, 47 (2013) 6691–6700.
- [13] H. Zhang, Y. Tian, L. Wang, L. Zhang, L. Dai, Ecophysiological characteristics and biogas production of cadmium-contaminated crops, *Bioresour. Technol.*, 146 (2013) 628–636.
- [14] K. Khan, Y. Lu, H. Khan, S. Zakir, S. Khan, A.A. Khan, L. Wei, T. Wang, Health risks associated with heavy metals in the drinking water of Swat, northern Pakistan, *J. Environ. Sci.*, 25 (2013) 2003–2013.
- [15] A.C. Davis, P. Wu, X. Zhang, X. Hou, B.T. Jones, Determination of cadmium in biological samples, *Appl. Spectrosc. Rev.*, 41 (2006) 35–75.
- [16] M. Tellez-Plaza, A. Navas-Acien, C.M. Crainiceanu, E. Guallar, Cadmium exposure and hypertension in the 1999–2004 National Health and Nutrition Examination Survey (NHANES), *Environ. Health Perspect.*, 116 (2008) 51–56.
- [17] D. Sud, G. Mahajan, M. Kaur, Agricultural waste material as potential adsorbent for sequestering heavy metal ions from aqueous solutions—a review, *Bioresour. Technol.*, 99 (2008) 6017–6027.
- [18] S.W. Won, P. Kotte, W. Wei, A. Lim, Y.-S. Yun, Biosorbents for recovery of precious metals, *Bioresour. Technol.*, 160 (2014) 203–212.
- [19] L.V.A. Gurgel, O.K. Junior, R.P. de Freitas Gil, L.F. Gil, Adsorption of $Cu(II)$, $Cd(II)$, and $Pb(II)$ from aqueous single metal solutions by cellulose and mercerized cellulose chemically modified with succinic anhydride, *Bioresour. Technol.*, 99 (2008) 3077–3083.

- [20] S. Prapagdee, S. Piyatiratitivorakul, A. Petsom, Activation of cassava stem biochar by physico-chemical method for stimulating cadmium removal efficiency from aqueous solution, *EnvironmentAsia*, 7 (2014) 60–69.
- [21] X. Yu, S. Tong, M. Ge, L. Wu, J. Zuo, C. Cao, W. Song, Adsorption of heavy metal ions from aqueous solution by carboxylated cellulose nanocrystals, *J. Environ. Sci.*, 25 (2013) 933–943.
- [22] M.A. Hussain, T.F. Liebert, Heinze, Alternative Routes of Polysaccharide Acylation: Synthesis, Structural Analysis, Properties, *Th. Polymer News*, 29 (2004) 14–17. Available at: <https://pdfs.semanticscholar.org/4fad/8c35e2df74ba9b1416a9228fc3e0e04dec9f.pdf>.
- [23] J.C. de Melo, E.C. da Silva Filho, S.A. Santana, C. Airoidi, Maleic anhydride incorporated onto cellulose and thermodynamics of cation-exchange process at the solid/liquid interface, *Colloids Surf., A*, 346 (2009) 138–145.
- [24] M.M. Zohourian, K. Kabiri, Superabsorbent polymer materials: a review, *Iran. Polym. J.*, 17 (2008) 451–447.
- [25] Z.Z. Summers, M. Aulton, M. Rubinstein, *Pharmaceutics: The Science of Dosage Form Design*, J. Am. Pharm. Inc., New York, 2007, pp. 70–98.
- [26] A. Suo, J. Qian, Y. Yao, W. Zhang, Synthesis and properties of carboxymethyl cellulose-graft-poly (acrylic acid-co-acrylamide) as a novel cellulose-based superabsorbent, *J. Appl. Polym.*, 103 (2007) 1382–1388.
- [27] S.A. Weerawarna, Method for Making Biodegradable Superabsorbent Particles, Google Patents, 2011.
- [28] F. Esposito, M.A. Del Nobile, G. Mensitieri, L. Nicolais, Water sorption in cellulose-based hydrogels, *J. Appl. Polym. Sci.*, 60 (1996) 2403–2407.
- [29] M.E. Aulton, *Pharmaceutics: The Science of Dosage Form Design*, Churchill Livingstone, Philadelphia, 2002, pp. 397–439.
- [30] S. Ring, Some studies on starch gelation, *Starch/Stärke*, 37 (1985) 80–83.
- [31] J. Peerapattana, P. Phuvarit, V. Srijesdaruk, D. Preechagoon, A. Tattawasart, Pregelatinized glutinous rice starch as a sustained release agent for tablet preparations, *Carbohydr. Polym.*, 80 (2010) 453–459.
- [32] E. Diez-Pena, I. Quijada-Garrido, J. Barrales-Rienda, On the water swelling behaviour of poly(N-isopropylacrylamide)[P (N-iPAAm)], poly(methacrylic acid)[P (MAA)], their random copolymers and sequential interpenetrating polymer networks (IPNs), *Polymers*, 43 (2002) 4341–4348.
- [33] M.K. Krušić, J. Filipović, Copolymer hydrogels based on N-isopropylacrylamide and itaconic acid, *Polymer*, 47 (2006) 148–155.
- [34] N. Peppas, B. Barr-Howell, Effect of Drug Loading Method and Drug Physicochemical Properties on the Materials, *Hydrogels in Medicine and Pharmacy*, Vol. 1, CRC Press, Boca Raton, FL, USA, 1986, pp. 27–56.
- [35] S. Ghasemi, M. Mousavi, M. Shamsipur, H. Karami, Sonochemical-assisted synthesis of nano-structured lead dioxide, *Ultrason. Sonochem.*, 15 (2008) 448–455.
- [36] C. Liu, R. Bai, Q. San Ly, Selective removal of copper and lead ions by diethylenetriamine-functionalized adsorbent: behaviors and mechanisms, *Water Res.*, 42 (2008) 1511–1522.